MATHEMATICS OF COMPUTATION
Volume 00, Number 0, Pages 000–000
S 0025-5718(XX)0000-0

C^2 HERMITE INTERPOLATION BY PYTHAGOREAN HODOGRAPH SPACE CURVES

ZBYNĚK ŠÍR AND BERT JÜTTLER

ABSTRACT. We solve the problem of C^2 Hermite interpolation by Pythagorean Hodograph (PH) space curves. More precisely, for any set of C^2 space boundary data (two points with associated first and second derivatives) we construct a four–dimensional family of PH interpolants of degree 9 and introduce a geometrically invariant parameterization of this family. This parameterization is used to identify a particular solution, which has the following properties. Firstly, it preserves planarity, i.e., the interpolant to planar data is a planar PH curve. Secondly, it has the best possible approximation order 6. Thirdly, it is symmetric in the sense that the interpolant of the "reversed" set of boundary data is simply the "reversed" original interpolant. This particular PH interpolant is exploited for designing algorithms for converting (possibly piecewise) analytical curves into a piecewise PH curve of degree 9 which is globally C^2, and for simple rational approximation of pipe surfaces with a piecewise analytical spine curve. The algorithms are presented along with an analysis of their error and approximation order.

1. INTRODUCTION

Pythagorean Hodograph (PH) curves (see the survey [12] and the references cited therein) form a remarkable subclass of polynomial parametric curves. They have a piecewise polynomial arc length function and, in the planar case, rational offset curves. These curves provide an elegant solution of various difficult problems occurring in applications, in particular in the context of CNC (computer-numerical-control) machining.

In the planar case, the properties and various constructions of PH curves have thoroughly been studied, e.g., [1, 7, 8, 9, 18, 25]. Due to the constrained nature of PH curves, all constructions – which are linear in the case of polynomial curves – become *nonlinear* in the PH case. Consequently, they may have more than one solution, and the problem of choosing the 'best' solution has to be addressed, e.g. by analyzing the approximation order or using the rotation index [18, 20, 22, 24].

Spatial PH curves were introduced by Farouki and Sakkalis in 1994 [6], and they have later been characterized using results about Pythagorean quadruples in the ring of polynomials and quaternion calculus [2, 4, 11]. Spatial PH curves are automatically equipped with rational frames, which were studied e.g. in [3, 14, 17].

Various constructions were also given, e.g. a global method for C^2 interpolation of point data by quintic splines has been presented in [13]. Hermite interpolation

1991 *Mathematics Subject Classification.* Primary 68U07; Secondary 53A04, 65D17.
Key words and phrases. Pythagorean Hodograph curves, Hermite interpolation, G-code, approximation order.

of G^1 boundary data was addressed in [17], and C^1 Hermite interpolation by PH quintics was discussed in [10, 23]. In the latter case, there exists a family of interpolants to any C^1 Hermite data which depends on two free parameters. Later, this result has also been related to helical interpolants [15].

The present paper is devoted to the problem of C^2 Hermite interpolation by spatial PH curves of degree 9 and it is organized as follows. First we recall some basic facts about quaternion algebra and PH curves. In the Section 3 we solve the C^2 interpolation problem and introduce a parameterization of the family of interpolants with respect to a standard position. We prove that this parameterization is geometrically invariant and symmetric. We also describe how C^2 Hermite interpolation in the plane is included in the spatial construction.

Section 4 provides a qualitative analysis of the solutions. We give an asymptotical analysis, including approximation order. Based on these results, in the Section 5 we use the "best" solution for converting analytical curves into piecewise PH quintic curves and for the approximation of pipe surfaces. Finally, we conclude the paper.

2. Preliminaries

First we recall some basic facts about quaternions and Pythagorean Hodograph curves.

2.1. **Quaternions.** Quaternions (see e.g. [19] for an elementary introduction) are elements

$$\mathcal{A} = a + a_x\mathbf{i} + a_y\mathbf{j} + a_z\mathbf{k} \tag{2.1}$$

of a 4–dimensional real linear space $\mathbb{Q}$ with basis $1, \mathbf{i}, \mathbf{j}, \mathbf{k}$. The space $\mathbb{Q}$ has the structure of a non-commutative field, where the multiplication is defined by the relations

$$\mathbf{i}^2 = \mathbf{j}^2 = \mathbf{k}^2 = \mathbf{ijk} = -1 \tag{2.2}$$

of the basis elements, which imply

$$\mathbf{ij} = -\mathbf{ji} = \mathbf{k}, \quad \mathbf{jk} = -\mathbf{kj} = \mathbf{i}, \quad \mathbf{ki} = -\mathbf{ik} = \mathbf{j}. \tag{2.3}$$

The conjugate of any quaternion (2.1) is defined as $\mathcal{A}^* = a - a_x\mathbf{i} - a_y\mathbf{j} - a_z\mathbf{k}$, and its absolute value is the non-negative real number

$$|\mathcal{A}| = \sqrt{\mathcal{A}\mathcal{A}^*} = \sqrt{\mathcal{A}^*\mathcal{A}} = \sqrt{a^2 + a_x^2 + a_y^2 + a_z^2}. \tag{2.4}$$

Unit quaternions, which are characterized by $|\mathcal{A}| = 1$, form a multiplicative group. We will use the notation

$$\mathcal{Q}(\phi) = (\cos\phi + \mathbf{i}\sin\phi) \tag{2.5}$$

for unit quaternions with vanishing $\mathbf{j}$ and $\mathbf{k}$ components.

Pure quaternions are distinguished by having a vanishing scalar part. In the sequel we will make use of the two following mappings.

Definition 2.1. We define mappings $\Xi_\theta, \Xi_\mathbf{k} : \mathbb{Q} \to \mathbb{Q}$ by

$$\Xi_\theta(\mathcal{A}) = \mathcal{Q}(\theta)\mathcal{A}\mathcal{Q}(-\theta), \text{ and } \Xi_\mathbf{k}(\mathcal{A}) = \mathbf{k}\mathcal{A}\mathbf{k}. \tag{2.6}$$

The mappings Ξ_θ, $\Xi_{\mathbf{k}}$ preserve pure quaternions and have the following geometrical meaning. Any vector $[a_x, a_y, a_z]^\top \in \mathbb{R}^3$ can be identified with the pure quaternion $a_x\mathbf{i} + a_y\mathbf{j} + a_z\mathbf{k}$. Then $\Xi_\theta : \mathbb{R}^3 \to \mathbb{R}^3$ is the rotation through the angle 2θ about the $\mathbf{i}$ axis and $\Xi_{\mathbf{k}} : \mathbb{R}^3 \to \mathbb{R}^3$ is the reflection with respect to the plane spanned by $\mathbf{i}$, $\mathbf{j}$.

Definition 2.2. We define on the quaternions the commutative multiplication

$$\mathcal{A} \star \mathcal{B} := \frac{1}{2}(\mathcal{A}\,\mathbf{i}\,\mathcal{B}^* + \mathcal{B}\,\mathbf{i}\,\mathcal{A}^*). \tag{2.7}$$

Corresponding n-th powers will be denoted $\mathcal{A}^{n\star} = \underbrace{\mathcal{A} \star \mathcal{A} \star \ldots \star \mathcal{A}}_{n\times}$.

Remark 2.3. Note, that $\mathcal{A} \star \mathcal{B}$ is in fact equal to the vector part of $\mathcal{A}\,\mathbf{i}\,\mathcal{B}^*$ and therefore is always a pure quaternion.

Lemma 2.4. *The multiplication $\star$ is invariant under mappings Ξ_θ and $\Xi_{\mathbf{k}}$, i.e. for any quaternions $\mathcal{A}$, $\mathcal{B}$*

$$\Xi_\theta(\mathcal{A} \star \mathcal{B}) = \Xi_\theta(\mathcal{A}) \star \Xi_\theta(\mathcal{B}) \quad \textit{and} \quad \Xi_{\mathbf{k}}(\mathcal{A} \star \mathcal{B}) = \Xi_{\mathbf{k}}(\mathcal{A}) \star \Xi_{\mathbf{k}}(\mathcal{B}). \tag{2.8}$$

Proof. The proof follows directly from the definitions.

$$\Xi_\theta(\mathcal{A}) \star \Xi_\theta(\mathcal{B}) = \frac{\mathcal{Q}(\theta)\mathcal{A}\mathcal{Q}(-\theta)\mathbf{i}\mathcal{Q}(\theta)\mathcal{B}^*\mathcal{Q}(-\theta) + \mathcal{Q}(\theta)\mathcal{B}\mathcal{Q}(-\theta)\mathbf{i}\mathcal{Q}(\theta)\mathcal{A}^*\mathcal{Q}(-\theta)}{2} =$$
$$= \mathcal{Q}(\theta)\frac{\mathcal{A}\mathbf{i}\mathcal{B}^* + \mathcal{B}\mathbf{i}\mathcal{A}^*}{2}\mathcal{Q}(-\theta) = \Xi_\theta(\mathcal{A} \star \mathcal{B}).$$

Similarly,

$$\Xi_{\mathbf{k}}(\mathcal{A}) \star \Xi_{\mathbf{k}}(\mathcal{B}) = \frac{\mathbf{k}\mathcal{A}\mathbf{k}\mathbf{i}(-\mathbf{k})\mathcal{B}^*(-\mathbf{k}) + \mathbf{k}\mathcal{B}\mathbf{k}\mathbf{i}(-\mathbf{k})\mathcal{A}^*(-\mathbf{k})}{2} =$$
$$= \mathbf{k}\frac{\mathcal{A}\mathbf{i}\mathcal{B}^* + \mathcal{B}\mathbf{i}\mathcal{A}^*}{2}\mathbf{k} = \Xi_{\mathbf{k}}(\mathcal{A} \star \mathcal{B}).$$

□

As we will see later, the solutions of the quaternion counterparts of quadratic and linear equations are essential for the construction of PH Hermite interpolants. We describe these solutions in the following lemmas.

Lemma 2.5. *Let $\mathbf{a}$ be a given pure quaternion and $\mathcal{B}$ a given non-zero quaternion. Then all solutions of the linear equation*

$$\mathcal{X} \star \mathcal{B} = \mathbf{a} \tag{2.9}$$

form the one–parameter family

$$\mathcal{X}_\tau = -\frac{(\tau + \mathbf{a})\,\mathcal{B}\,\mathbf{i}}{|\mathcal{B}|^2} \quad \textit{with the parameter } \tau \in \mathbb{R}. \tag{2.10}$$

Moreover this parameterization of the system of solutions is compatible with the mappings Ξ_θ and $\Xi_{\mathbf{k}}$ in the following way. If $\tilde{\mathcal{A}}_\tau$ denotes the solutions for the data transformed by Ξ_θ and $\bar{\mathcal{A}}_\tau$ for the data transformed by $\Xi_{\mathbf{k}}$, then for any τ

$$\tilde{\mathcal{A}}_\tau = \Xi_\theta(\mathcal{A}_\tau) \textit{ and } \bar{\mathcal{A}}_\tau = \Xi_{\mathbf{k}}(\mathcal{A}_{-\tau}). \tag{2.11}$$

Proof. Due to Remark 2.3, Eq. (2.9) is equivalent to $\mathcal{A}\mathbf{i}\mathcal{B}^* = \tau + \mathbf{a}$ for some $\tau \in \mathbb{R}$, which is a simple modification of (2.10). Moreover for any fixed value of τ we have

$$\tilde{\mathcal{X}}_\tau = -\frac{[\tau + \Xi_\theta(\mathbf{a})]\,\Xi_\theta(\mathcal{B})\,\mathbf{i}}{|\Xi_\theta(\mathcal{B})|^2} = -\frac{\Xi_\theta(\tau+\mathbf{a})\,\Xi_\theta(\mathcal{B})\,\Xi_\theta(\mathbf{i})}{|\mathcal{B}|^2} = \Xi_\theta\left(-\frac{(\tau+\mathbf{a})\,\mathcal{B}\,\mathbf{i}}{|\mathcal{B}|^2}\right) = \Xi_\theta(\mathcal{X}_\tau)$$

and

$$\bar{\mathcal{X}}_\tau = -\frac{[\tau + \Xi_{\mathbf{k}}(\mathbf{a})]\,\Xi_{\mathbf{k}}(\mathcal{B})\,\mathbf{i}}{|\Xi_{\mathbf{k}}(\mathcal{B})|^2} = -\frac{(\tau+\mathbf{k}\mathbf{a}\mathbf{k})\,(\mathbf{k}\mathcal{B}\mathbf{k})\,\mathbf{i}}{|\mathbf{k}\mathcal{B}\mathbf{k}|^2} = \mathbf{k}\left(-\frac{(-\tau+\mathbf{a})\,\mathcal{B}\,\mathbf{i}}{|\mathcal{B}|^2}\right)\mathbf{k} = \Xi_{\mathbf{k}}(\mathcal{X}_{-\tau}).$$

□

Lemma 2.6. *Let* $\mathbf{a}$ *be a given pure quaternion, which is not a negative multiple of* $\mathbf{i}$*. Then all solutions of the quadratic equation*

$$\mathcal{X}^{2\star} = \mathbf{a} \tag{2.12}$$

form the one–parameter family

$$\mathcal{X}_\phi = \sqrt{|\mathbf{a}|}\,\frac{\frac{\mathbf{a}}{|\mathbf{a}|}+\mathbf{i}}{\left|\frac{\mathbf{a}}{|\mathbf{a}|}+\mathbf{i}\right|}\,\mathcal{Q}(\phi), \quad \text{with the parameter } \phi \in [0, 2\pi). \tag{2.13}$$

Moreover this parameterization of the system of solutions is compatible with the mappings Ξ_θ *and* $\Xi_{\mathbf{k}}$ *in the following way. If* $\tilde{\mathcal{X}}(\phi)$ *denotes the solutions for the data transformed by* Ξ_θ *and* $\bar{\mathcal{X}}(\phi)$ *for the data transformed by* $\Xi_{\mathbf{k}}$*, then for any* ϕ

$$\tilde{\mathcal{X}}_\phi = \Xi_\theta(\mathcal{X}_\phi) \text{ and } \bar{\mathcal{X}}_\phi = \Xi_{\mathbf{k}}(\mathcal{X}_{-\phi}). \tag{2.14}$$

Proof. The formula (2.13) is given with a proof in [10, section 3.2]. For the proof of invariance consider that

$$\begin{aligned}\tilde{\mathcal{X}}_\phi &= \sqrt{|\Xi_\theta(\mathbf{a})|}\,\frac{\frac{\Xi_\theta(\mathbf{a})}{|\Xi_\theta(\mathbf{a})|}+\mathbf{i}}{\left|\frac{\Xi_\theta(\mathbf{a})}{|\Xi_\theta(\mathbf{a})|}+\mathbf{i}\right|}\,\mathcal{Q}(\phi) = \sqrt{|\mathbf{a}|}\,\frac{\Xi_\theta\left(\frac{\mathbf{a}}{|\mathbf{a}|}+\mathbf{i}\right)}{\left|\frac{\mathbf{a}}{|\mathbf{a}|}+\mathbf{i}\right|}\,\Xi_\theta\left(\mathcal{Q}(\phi)\right)\\ &= \Xi_\theta\left(\sqrt{|\mathbf{a}|}\,\frac{\frac{\mathbf{a}}{|\mathbf{a}|}+\mathbf{i}}{\left|\frac{\mathbf{a}}{|\mathbf{a}|}+\mathbf{i}\right|}\,\mathcal{Q}(\phi)\right) = \Xi_\theta(\mathcal{X}_\phi).\end{aligned} \tag{2.15}$$

Similarly, due to $\mathbf{kik} = \mathbf{i}$ and $\mathbf{k}\mathcal{Q}(\phi) = \mathcal{Q}(-\phi)\mathbf{k}$,

$$\tilde{\mathcal{X}}_\phi = \sqrt{|\Xi_{\mathbf{k}}(\mathbf{a})|}\,\frac{\frac{\Xi_{\mathbf{k}}(\mathbf{a})}{|\Xi_{\mathbf{k}}(\mathbf{a})|}+\mathbf{i}}{\left|\frac{\Xi_{\mathbf{k}}(\mathbf{a})}{|\Xi_{\mathbf{k}}(\mathbf{a})|}+\mathbf{i}\right|}\,\mathcal{Q}(\phi) = \mathbf{k}\left(\sqrt{|\mathbf{a}|}\,\frac{\frac{\mathbf{a}}{|\mathbf{a}|}+\mathbf{i}}{\left|\frac{\mathbf{a}}{|\mathbf{a}|}+\mathbf{i}\right|}\right)\mathbf{k}\,\mathcal{Q}(\phi) = \Xi_{\mathbf{k}}(\mathcal{X}_{-\phi}). \tag{2.16}$$

□

Definition 2.7. The set of all quaternions of the form $a\mathbf{i} + b\mathbf{j}$, $a, b \in \mathbb{R}$ will be denoted by $\mathbb{Q}_{\mathbf{ij}}$.

The following lemma can be verified directly:

Lemma 2.8. $\mathbb{Q}_{\mathbf{ij}}$ *is preserved by the multiplication* $\star$*. Moreover* $\mathbb{Q}_{\mathbf{ij}}$ *together with the multiplication* $\star$ *and the standard addition is isomorphic to the field of complex numbers.*

Lemma 2.9. *If* $\mathcal{B}, \mathbf{a} \in \mathbb{Q}_{\mathbf{ij}}$*, then*

1. $\mathcal{X}_0$ *is the only solution of Eq.* (2.9) *which is contained in* $\mathbb{Q}_{\mathbf{ij}}$*.*
2. $\mathcal{X}_0$ *and* $\mathcal{X}_\pi$ *are the only solutions of Eq.* (2.12) *which are contained in* $\mathbb{Q}_{\mathbf{ij}}$*.*

Proof. The results can be proved in a straightforward way by expressing $\mathcal{B}$ and $\mathbf{a}$ using their $\mathbf{i}$ and $\mathbf{j}$ parts. □

2.2. **Pythagorean Hodograph curves.** The *hodograph* of a space curve $\mathbf{p}(t) = [x(t), y(t), z(t)]^\top$ of degree n is the curve $\mathbf{h}(t) = [x'(t), y'(t), z'(t)]^\top$ of degree $n-1$, where $'$ denotes the first derivative. Recall that a polynomial curve is called *Pythagorean Hodograph (PH)*, if the length of its tangent vector depends in a (piecewise) polynomial way on the parameter. In particular, $\mathbf{p}(t) = [x(t), y(t), z(t)]^\top$ is called *space PH curve* if there exists a polynomial $\sigma(t)$ such that

$$x'(t)^2 + y'(t)^2 + z'(t)^2 = \sigma^2(t). \tag{2.17}$$

If all real roots of $\gcd(x'(t), y'(t), z'(t))$ have even multiplicity [1], then equation (2.17) holds if and only if there exist polynomials $u(t), v(t), p(t), q(t)$ such that

$$\begin{aligned} x'(t) &= u^2(t) + v^2(t) - p^2(t) - q^2(t), \\ y'(t) &= 2u(t)q(t) + 2v(t)p(t), \\ z'(t) &= 2v(t)q(t) - 2u(t)p(t), \\ \sigma(t) &= u^2(t) + v^2(t) + p^2(t) + q^2(t), \end{aligned} \tag{2.18}$$

see [4]. This result can be reformulated using quaternions [2, 11]. Any spatial polynomial curve $\mathbf{p}(t) = [x(t), y(t), z(t)]^\top$ is identified with the pure–quaternion–valued function $\mathbf{p}(t) = x(t)\mathbf{i} + y(t)\mathbf{j} + z(t)\mathbf{k}$. The PH curves are then characterized as follows.

Lemma 2.10. *Let* $\mathbf{p}(t) = x(t)\mathbf{i}+y(t)\mathbf{j}+z(t)\mathbf{k}$ *be a space polynomial curve, such that all real roots of* $\gcd(x'(t), y'(t), z'(t))$ *have even multiplicity. Then* $\mathbf{p}(t)$ *is PH if and only if there exists a quaternion-valued polynomial* $\mathcal{A}(t) = u(t)+v(t)\mathbf{i}+p(t)\mathbf{j}+q(t)\mathbf{k}$ *such that*

$$\mathbf{h}(t) = \mathcal{A}(t)\,\mathbf{i}\,\mathcal{A}^*(t) = \mathcal{A}(t)^{2\star} \tag{2.19}$$

The arc length function of the PH curve is a polynomial obtained by integrating $|\mathcal{A}(t)|^2 = \mathcal{A}(t)\mathcal{A}^*(t)$.

Consequently, the construction of a PH curve is reduced to the construction of a suitable curve $\mathcal{A}(t)$. This curve will be called the *preimage*.

Remark 2.11. The general form of the hodograph of a PH curve (without imposing the condition concerning the common factors in Lemma 2.10) is

$$\mathbf{h}(t) = (t-t_1)(t-t_2)\dots(t-t_k)A(t)^{2\star}, \tag{2.20}$$

where t_i are distinct real numbers [2]. However, the common factors $(t-t_i)$ raise the degree of the curve without yielding more geometric flexibility (they do not modify tangent directions) and moreover they introduce cusps at parameter values t_i, which can be in the region of interest (see Figure 2). For this reason these "spurious" solutions are not likely to be useful for applications and we will omit them in the remainder of the paper.

[1] This includes the generic case $\gcd(x'(t), y'(t), z'(t)) = 1$.

2.3. **Pythagorean Hodograph curves of degree 9.** In the sequel we will use PH curves of degree 9. The PH curves, their hodograph $\mathbf{h}(t) = \mathbf{p}'(t)$ and the preimage $\mathcal{A}(t)$ will be expressed in the Bernstein-Bézier representation [16]

(2.21)
$$\mathbf{p}(t) = \sum_{i=0}^{9} \mathbf{p}_i B_i^9(t), \quad \mathbf{h}(t) = \sum_{i=0}^{8} \mathbf{h}_i B_i^8(t), \quad \mathcal{A}(t) = \sum_{i=0}^{4} \mathcal{A}_i B_i^4(t), \quad t \in [0,1],$$

where $\mathbf{p}_i$, $\mathbf{h}_i$ (pure quaternions) and $\mathcal{A}_i$ (quaternions) are the control points and $B_j^n(t) = \binom{n}{j} t^j (1-t)^{n-j}$ are the Bernstein polynomials. The relation between the hodograph and the preimage

$$\mathbf{h}(t) = \mathcal{A}(t)^{2\star} \tag{2.22}$$

can be expressed using the control points as

$$\mathbf{h}_0 = \mathcal{A}_0^{2\star} \tag{2.23}$$
$$\mathbf{h}_1 = \mathcal{A}_0 \star \mathcal{A}_1 \tag{2.24}$$
$$\mathbf{h}_2 = (4\mathcal{A}_1^{2\star} + 3\mathcal{A}_0 \star \mathcal{A}_2)/7 \tag{2.25}$$
$$\mathbf{h}_3 = (\mathcal{A}_0 \star \mathcal{A}_3 + 6\mathcal{A}_1 \star \mathcal{A}_2)/7 \tag{2.26}$$
$$\mathbf{h}_4 = (18\mathcal{A}_2^{2\star} + \mathcal{A}_0 \star \mathcal{A}_4 + 16\mathcal{A}_1 \star \mathcal{A}_3)/35 \tag{2.27}$$
$$\mathbf{h}_5 = (\mathcal{A}_1 \star \mathcal{A}_4 + 6\mathcal{A}_2 \star \mathcal{A}_3)/7 \tag{2.28}$$
$$\mathbf{h}_6 = (4\mathcal{A}_3^{2\star} + 3\mathcal{A}_2 \star \mathcal{A}_4)/7 \tag{2.29}$$
$$\mathbf{h}_7 = A_3 \star \mathcal{A}_4 \tag{2.30}$$
$$\mathbf{h}_8 = \mathcal{A}_4^{2\star}. \tag{2.31}$$

The PH curve is obtained by integrating the hodograph and it possesses the control points

$$\mathbf{p}_j = \mathbf{p}_0 + \frac{1}{9} \sum_{i=0}^{j-1} \mathbf{h}_i, \quad j = 1, \ldots, 9. \tag{2.32}$$

3. C^2 Hermite interpolation

We construct a spatial PH curve $\mathbf{p}(t)$ which matches given C^2 Hermite boundary data. More precisely, the curve is to interpolate the end points $\mathbf{p}_b$, $\mathbf{p}_e$, the first derivative vectors (velocities) $\mathbf{v}_b$, $\mathbf{v}_e$ and the second derivative vectors (accelerations) $\mathbf{a}_b$, $\mathbf{a}_e$.

In all we have 18 scalar conditions. Three of them are satisfied by choosing the first control point of the curve $\mathbf{p}_0 = \mathbf{p}_b$. The remaining 15 conditions must be satisfied by determining the control points of the preimage. As the preimage has 4 components (quaternions), apparently the 15 conditions could be satisfied by 4 control points leading to the preimage of degree 3 and PH curves of degree 7. But our experiments showed, that the resulting system of equations is highly nonlinear and does not have solutions for all input data - see section 3.4. Therefore we will use PH interpolants of degree 9, for which the problem always has solutions forming a 4 parameter family.

3.1. **Construction of the interpolants.** Two curves $\mathbf{p}(t)$, $\tilde{\mathbf{p}}(t)$ share the same hodograph if and only if they differ only by a translation. Consequently, a space PH curve $\mathbf{p}(t)$ is fully determined by the preimage $\mathcal{A}(t)$ and by the location of its starting point $\mathbf{p}(0)$.

Using the curves of degree 9, the interpolation conditions lead to the equations

$$\mathbf{h}_0 = \mathbf{v}_b,\ \mathbf{h}_8 = \mathbf{v}_e,\ 8(\mathbf{h}_1 - \mathbf{h}_0) = \mathbf{a}_b,\ 8(\mathbf{h}_8 - \mathbf{h}_7) = \mathbf{a}_e, \tag{3.1}$$

$$\frac{1}{9}\sum_{i=0}^{8} \mathbf{h}_i = (\mathbf{p}_e - \mathbf{p}_b). \tag{3.2}$$

Substituting into (2.23)–(2.31) we get after some simplifications

(3.3)

$$\begin{aligned}(12\mathcal{A}_2 + 10\mathcal{A}_1 + 5\mathcal{A}_0 + 5\mathcal{A}_4 + 10\mathcal{A}_3)^{2\star} = \\ 2520(\mathbf{p}_e - \mathbf{p}_b) - 435(\mathbf{v}_e + \mathbf{v}_b) + \tfrac{45}{2}(\mathbf{a}_e - \mathbf{a}_b) \\ -(60\mathcal{A}_1^{2\star} - 60\mathcal{A}_0 \star \mathcal{A}_3 - 60\mathcal{A}_1 \star \mathcal{A}_4 + 60\mathcal{A}_3^{2\star} - 42\mathcal{A}_0 \star \mathcal{A}_4 - 72\mathcal{A}_1 \star \mathcal{A}_3).\end{aligned}$$

Algorithm 3.1 (Construction of PH interpolants)**.**

1. Compute the control points $\mathbf{h}_0$, $\mathbf{h}_1$, $\mathbf{h}_7$ and $\mathbf{h}_8$ from the equations (3.1).
2. The control points $\mathcal{A}_0$, $\mathcal{A}_4$ can be computed from the equations (2.23), (2.31), which are of type (2.12) and therefore each of $\mathcal{A}_0$, $\mathcal{A}_4$ depends on one free parameter, say on θ_0 and θ_4.
3. The control points $\mathcal{A}_1$, $\mathcal{A}_3$ can be computed from equations (2.24), (2.30), which are of type (2.9). The control point $\mathcal{A}_1$ depends on the parameter θ_0 via the point $\mathcal{A}_0$ and on a new parameter τ_1. Similarly $\mathcal{A}_3$ depends on the parameter θ_4 via the point $\mathcal{A}_4$ and on a new parameter τ_3.
4. The control point $\mathcal{A}_2$ can be computed from (3.3), which is essentially of type (2.12). This control point will depend on all previous control points and therefore on all parameters θ_0, θ_4, τ_1 and τ_3 and on a new parameter θ_2.
5. Compute control points $\mathbf{h}_2$, $\mathbf{h}_3$, $\mathbf{h}_4$, $\mathbf{h}_5$, $\mathbf{h}_6$ from equations (2.25)–(2.29), set $\mathbf{p}_0 = \mathbf{p}_b$ and compute the remaining control points of $\mathbf{p}(t)$ from the equation (2.32).

Summing up, we arrive successively at families of suitable preimages $\mathcal{A}_\Phi(t)$, hodographs $\mathbf{h}_\Phi(t)$ and PH curves $\mathbf{p}_\Phi(t)$ depending on parameter vectors $\Phi = [\theta_0, \tau_1, \theta_2, \tau_3, \theta_4]$.

Remark 3.2. Let us make more explicit the step 4 of the Algorithm 3.1. Denoting the right-hand side of the equation (3.3) by $\mathbf{r}_\Phi$ and using Lemma (2.6) we obtain the control point $\mathcal{A}_2$ depending on Φ:

$$\mathcal{A}_2 = \frac{1}{12}\left(\sqrt{|\mathbf{r}_\Phi|}\,\frac{\frac{\mathbf{r}_\Phi}{|\mathbf{r}_\Phi|} + \mathbf{i}}{\left|\frac{\mathbf{r}_\Phi}{|\mathbf{r}_\Phi|} + \mathbf{i}\right|}\mathcal{Q}(\theta_2) - 10\mathcal{A}_1 - 5\mathcal{A}_0 - 5\mathcal{A}_4 - 10\mathcal{A}_3\right). \tag{3.4}$$

As in the case of the C^1 Hermite interpolation [10, 23], one of the angular parameters, say θ_2, can be chosen to be zero due to the nontrivial fibers of the mapping *preimage* $\rightarrow$ *hodograph* (2.19). This fact is formally proved in the following lemma.

Lemma 3.3. *If two parameter vectors differ only by the same angle for the three angular parameters*

$$\Phi = [\theta_0, \tau_1, \theta_2, \tau_3, \theta_4] \quad \textit{and} \quad \tilde{\Phi} = [\theta_0 + \alpha, \tau_1, \theta_2 + \alpha, \tau_3, \theta_4 + \alpha],$$

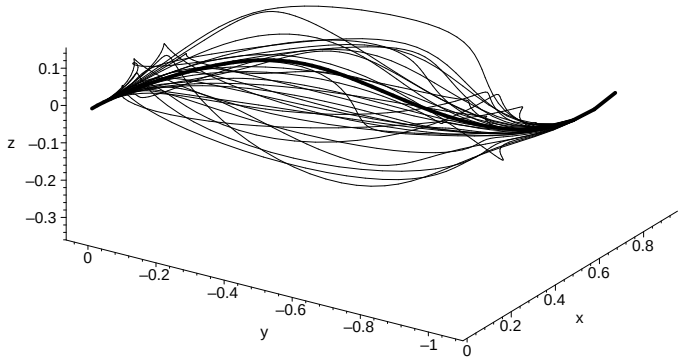

FIGURE 1. 32 representants of the four dimensional system of PH interpolants of the data (3.9). The "best" interpolant (see Theorem 4.2) is plotted in bold.

then $\mathbf{h}_\Phi(t) = \mathbf{h}_{\tilde{\Phi}}(t)$ *and therefore also* $\mathbf{p}_\Phi(t) = \mathbf{p}_{\tilde{\Phi}}(t)$.

Proof. Let $\mathcal{A}_i, \mathbf{h}_i$ and $\tilde{\mathcal{A}}_i, \tilde{\mathbf{h}}_i$ denote the control points constructed with parameters Φ and $\tilde{\Phi}$, respectively. Considering the step 2 of the Algorithm 3.1 we have

$$\tilde{\mathcal{A}}_0 = \mathcal{A}_0 \mathcal{Q}(\alpha) \quad \text{and} \quad \tilde{\mathcal{A}}_4 = \mathcal{A}_4 \mathcal{Q}(\alpha). \tag{3.5}$$

In step 3 we get

$$\tilde{\mathcal{A}}_1 = -\frac{(\tau + \mathbf{h}_1)\, \mathcal{B}\mathcal{Q}(\alpha)\, \mathbf{i}}{|\mathcal{B}\mathcal{Q}(\alpha)|^2} = -\frac{(\tau + \mathbf{h}_1)\, \mathcal{B}\, \mathbf{i}}{|\mathcal{B}|^2}\, \mathcal{Q}(\alpha) = \mathcal{A}_1 \mathcal{Q}(\alpha) \tag{3.6}$$

and in a similar way $\tilde{\mathcal{A}}_3 = \mathcal{A}_3 \mathcal{Q}(\alpha)$. Finally, due to the fact that for any $\mathcal{X}$, $\mathcal{Y}$

$$[\mathcal{X}\mathcal{Q}(\alpha)] \star [\mathcal{Y}\mathcal{Q}(\alpha)] = \mathcal{X} \star \mathcal{Y} \tag{3.7}$$

holds, we have $\mathbf{r}_\Phi = \mathbf{r}_{\tilde{\Phi}}$ (see Remark 3.2) and therefore $\tilde{\mathcal{A}}_2 = \mathcal{A}_2 \mathcal{Q}(\alpha)$. So, for the whole preimage, $\tilde{\mathcal{A}}(t) = \mathcal{A}\mathcal{Q}(\alpha)$ holds. Finally, (3.7) implies

$$\tilde{\mathbf{h}}(t) = \mathbf{h}(t). \tag{3.8}$$

□

Remark 3.4. As a consequence, all PH interpolants can be obtained using parameter vectors with $\theta_2 = 0$. In the remainder of the paper we will suppose this choice and we will omit θ_2 in the parameter vector Φ, which will be now written as $\Phi = [\theta_0, \tau_1, \tau_3, \theta_4]$.

Example 3.5. For any C^2 Hermite data we thus obtain a four dimensional system of PH interpolants of degree 9. As a first example, Figure 1 shows the system of PH interpolants to the data

(3.9)

$$\begin{array}{lllllllll} \mathbf{p}_b & = & [0,0,0], & \mathbf{v}_b & = & [\frac{10}{9},0,0], & \mathbf{a}_b & = & [\frac{25}{6},-\frac{10}{3},0] \\ \mathbf{p}_e & = & [\frac{89}{126},-\frac{68}{63},\frac{5}{126}], & \mathbf{v}_e & = & [-\frac{20}{9},-\frac{40}{9},\frac{40}{9}], & \mathbf{a}_e & = & [-\frac{65}{3},-10,\frac{170}{3}]. \end{array}$$

In addition to the C^2 interpolants constructed using the Algorithm 3.1, there may exist so–called "spurious" PH interpolants of degree 9 (see Remark 2.11). Figure 2 shows one of these interpolants to the data (3.9), having two cusps in the

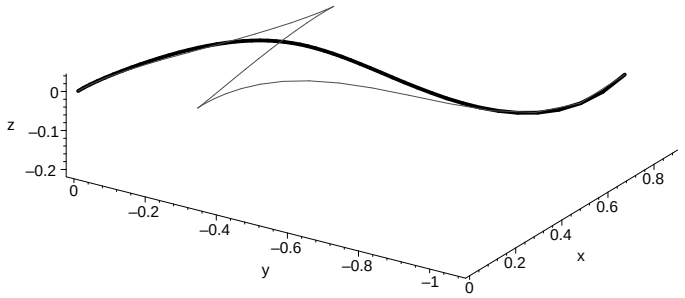

FIGURE 2. An example of a spurious interpolant of the data (3.9) together with the "best" interpolant (see Theorem 4.2).

region of interest. In the sequel we will ignore this kind of interpolants and will restrict ourselves only to those constructed by the Algorithm 3.1.

3.2. **Invariance of interpolants.** Considered as a set, the system $\{\mathbf{p}_\Phi(t)\}$ of PH interpolants of some Hermite data is invariant with respect to orthogonal transformations (including reflections). More precisely, if we apply an orthogonal transformation Ξ to the Hermite data, we get modified data $\tilde{\mathbf{p}}_b$, $\tilde{\mathbf{p}}_e$, $\tilde{\mathbf{v}}_b$, $\tilde{\mathbf{v}}_e$, $\tilde{\mathbf{a}}_b$, $\tilde{\mathbf{a}}_e$. The associated systems of interpolants satisfy

$$\{\tilde{\mathbf{p}}_\Phi(t)\} = \Xi(\{\mathbf{p}_\Phi(t)\}).$$

On the other hand, this transformation does not preserve the parameterization of the solutions: In general

$$\tilde{\mathbf{p}}_{\tilde{\Phi}}(t) = \Xi(\mathbf{p}_\Phi(t)) \tag{3.10}$$

is not valid for $\tilde{\Phi} = \Phi$.

The relation between $\tilde{\Phi}$ and Φ ensuring (3.10) is rather complicated. Still, it can be formulated easily in the following cases.

Lemma 3.6. *For any Φ:*

(1) *If Ξ_θ is a rotation about the* **i***-axis, then*

$$\tilde{\mathbf{p}}_\Phi(t) = \Xi_\theta(\mathbf{p}_\Phi(t)).$$

(2) *If $\Xi_{\mathbf{k}}$ is the reflection with respect to the* **ij** *plane, then*

$$\tilde{\mathbf{p}}_\Phi(t) = \Xi_{\mathbf{k}}(\mathbf{p}_{-\Phi}(t)).$$

Proof. Consider a fixed parameter vector Φ and let $\mathcal{A}_i$ denote the control points of the preimage for some data $\mathbf{p}_b$, $\mathbf{p}_e$, $\mathbf{v}_b$, $\mathbf{v}_e$, $\mathbf{a}_b$, $\mathbf{a}_e$ and $\tilde{\mathcal{A}}_i$ for the transformed data $\tilde{\mathbf{p}}_b = \Xi_\theta(\mathbf{p}_b)$, $\tilde{\mathbf{p}}_e = \Xi_\theta(\mathbf{p}_e)$, $\tilde{\mathbf{v}}_b = \Xi_\theta(\mathbf{v}_b)$, $\tilde{\mathbf{v}}_e = \Xi_\theta(\mathbf{v}_e)$, $\tilde{\mathbf{a}}_b = \Xi_\theta(\mathbf{a}_b)$, $\tilde{\mathbf{a}}_e = \Xi_\theta(\mathbf{a}_e)$.

1) Due to Lemma 2.6 we have in the step 2 of the Algorithm 3.1

$$\tilde{\mathcal{A}}_0 = \Xi_\theta(\mathcal{A}_0) \text{ and } \tilde{\mathcal{A}}_4 = \Xi_\theta(\mathcal{A}_4). \tag{3.11}$$

Then due to Lemma 2.5 we have in the step 3

$$\tilde{\mathcal{A}}_1 = \Xi_\theta(\mathcal{A}_1) \text{ and } \tilde{\mathcal{A}}_3 = \Xi_\theta(\mathcal{A}_3). \tag{3.12}$$

Finally, in step 4, we have $\tilde{\mathbf{r}}_\Phi = \Xi_\theta(\mathbf{r}_\Phi)$, due to Lemma 2.4. Hence, $\tilde{\mathcal{A}}_3 = \Xi_\theta(\mathcal{A}_3)$ and thus for the whole preimage curve $\tilde{\mathcal{A}}(t) = \Xi_\theta(\mathcal{A}(t))$. Finally due to Lemma 2.4 we obtain in step 5 $\tilde{\mathbf{p}}_i = \Xi_\theta(\mathbf{p}_i)$ and therefore $\tilde{\mathbf{p}}(t) = \Xi_\theta(\mathbf{p}(t))$.

2) Due to the same lemmas, the previous argument holds also for $\Xi_{\mathbf{k}}$ if the control points $\tilde{\mathcal{A}}_i$ are constructed with parameters $-\Phi$, while the control points $\mathcal{A}_i$ are constructed with the parameters Φ. □

A fully invariant parameterization of interpolants is obtained by considering a standard position.

Definition 3.7. The given C^2 spatial Hermite data are said to be in a standard position if $\mathbf{v}_b + \mathbf{v}_e$ is a positive multiple of $\mathbf{i}$ and $\mathbf{p}_b = 0$.

This choice of standard position express an "algebraic symmetry" of the data and therefore allows a simple identification of the symmetric solution in the Theorem 3.10. Moreover it is very simple from the computational point of view. Other definitions of a standard position would be possible. For instance one could require the $\mathbf{i}$-axis to be the bisector of the angle between the vectors $\mathbf{v}_b$ and $\mathbf{v}_e$, or $\mathbf{p}_e - \mathbf{p}_b$ to be a positive multiple of $\mathbf{i}$.

From now on, we will use the following parameterization of the system of interpolants.

Definition 3.8. The system of interpolants is parameterized by the parameters Φ as follows. Firstly, we transform the data to a standard position by a rotation and translation. Secondly, we construct the interpolants $\mathbf{p}_\Phi$, as described before. Finally, we transform the solution back to the original position.

Note that parameterization is well–defined, since Lemma 3.6 ensures that the particular choice of a standard position (which may vary by a rotation about $\mathbf{i}$ axis) does not matter.

The only case in which the Definition 3.8 fails is that of "antipodal" velocities $\mathbf{v}_b + \mathbf{v}_e = 0$. This case will not be analyzed in detail, since it can be avoided in subdivision-based algorithms by using a sufficiently small stepsize (see Section 5). However, the parameterization defined in Definition 3.8 can be extended to the case $\mathbf{v}_b + \mathbf{v}_e = 0$, but not in a continuous way. The discontinuity in the parameterization of the interpolants turns out to be an inevitable feature, as explained in more detail for the planar case in [22].

Theorem 3.9. *The parameterization of the solutions, according to Definition 3.8, is invariant with respect to rigid body motions (special orthogonal transformations), whereas reflections change the signs of all parameters. Consequently, the interpolant obtained for $\Phi = [0, 0, 0, 0]$ is invariant with respect to all orthogonal transformations.*

The proof results from Lemma 3.6.

In addition, the parameterization of the solutions is symmetric with respect to swapping the "direction" or the given data in the following sense.

Theorem 3.10. *Let $\mathbf{p}_\Phi(t)$ be the interpolants of data $\mathbf{p}_b, \mathbf{p}_e, \mathbf{v}_b, \mathbf{v}_e, \mathbf{a}_b, \mathbf{a}_e$ and $\bar{\mathbf{p}}_\Phi(t)$ the interpolants of the "reversed" data*

$$\bar{\mathbf{p}}_b = \mathbf{p}_e,\ \bar{\mathbf{p}}_e = \mathbf{p}_b,\ \bar{\mathbf{v}}_b = -\mathbf{v}_e,\ \bar{\mathbf{v}}_e = -\mathbf{v}_b,\ \bar{\mathbf{a}}_b = \mathbf{a}_e,\ \bar{\mathbf{a}}_e = \mathbf{a}_b, \tag{3.13}$$

respectively. Then for any parameter vector $\Phi = [\theta_0, \tau_1, \tau_3, \theta_4]$ *we have*

$$\bar{\mathbf{p}}_{[\theta_0,\tau_1,\tau_3,\theta_4]}(1-t) = \mathbf{p}_{[-\theta_4,-\tau_3,-\tau_1,-\theta_0]}(t). \tag{3.14}$$

Consequently, the solutions $\mathbf{p}_{[0,0,0,0]}$ *and* $\bar{\mathbf{p}}_{[0,0,0,0]}$ *are identical.*

Proof. Suppose that the given data are in a standard position, i.e. $\mathbf{v}_b + \mathbf{v}_e$ is a positive multiple of $\mathbf{i}$ and $\mathbf{p}_b = 0$. Then the reversed data (3.13) are not in a standard position, but applying the translation by the vector $-\mathbf{p}_e$ and the symmetry $S : \mathbf{c} \to -\mathbf{c}$ we obtain new data

$$\tilde{\mathbf{p}}_b = 0,\ \tilde{\mathbf{p}}_e = \mathbf{p}_e,\ \tilde{\mathbf{v}}_b = \mathbf{v}_e,\ \tilde{\mathbf{v}}_e = \mathbf{v}_b,\ \tilde{\mathbf{a}}_b = -\mathbf{a}_e,\ \tilde{\mathbf{a}}_e = -\mathbf{a}_b, \tag{3.15}$$

which are in a standard position. Now using the Algorithm 3.1 we obtain in step 1

$$\begin{gathered} \tilde{\mathbf{h}}_0 = \tilde{\mathbf{v}}_b = \mathbf{v}_e = \mathbf{h}_8, \quad \tilde{\mathbf{h}}_8 = \tilde{\mathbf{v}}_e = \mathbf{v}_b = \mathbf{h}_0 \\ \tilde{\mathbf{h}}_1 = \frac{\tilde{\mathbf{a}}_b}{8} + \tilde{\mathbf{h}}_0 = -\frac{\mathbf{a}_e}{8} + \mathbf{h}_8 = \mathbf{h}_7, \quad \tilde{\mathbf{h}}_7 = -\frac{\tilde{\mathbf{a}}_e}{8} + \tilde{\mathbf{h}}_8 = \frac{\mathbf{a}_b}{8} + \mathbf{h}_0 = \mathbf{h}_1. \end{gathered} \tag{3.16}$$

Due to the symmetry of the construction of the control points $\mathbf{h}_i$, and $\mathbf{h}_{8-i}$ in the steps 1-3 of the Algorithm 3.1, we obtain $\tilde{\mathbf{h}}_{[\theta_0,\tau_1,\tau_3,\theta_4]}(1-t) = \mathbf{h}_{[\theta_4,\tau_3,\tau_1,\theta_0]}(t)$ and therefore also

$$\tilde{\mathbf{p}}_{[\theta_0,\tau_1,\tau_3,\theta_4]}(1-t) = \mathbf{p}_{[\theta_4,\tau_3,\tau_1,\theta_0]}(t). \tag{3.17}$$

The data (3.15) are in a standard position, which is not associated with the reversed data (3.13) according to the definition 3.8, since they differ not by a rotation, but by the symmetry S changing orientation. A standard position associated with the reversed data (3.13) can be obtained from the data (3.15) applying additional reflection $\Xi_{\mathbf{k}}$ (2.6). Then following lemma 3.6 (2) we have $\bar{\mathbf{p}}_{[\theta_0,\tau_1,\tau_3,\theta_4]} = \tilde{\mathbf{p}}_{[-\theta_0,-\tau_1,-\tau_3,-\theta_4]}$ and together with (3.17) we obtain (3.14). □

3.3. **The case of planar data.** As a natural question, one may ask whether the PH interpolants $\mathbf{p}_\Phi$ of C^2 Hermite data lying in a plane P are planar. Our experiments show that this is not the case. Due to the C^2 conditions, the 6 control points (three extremal points at each side) of all interpolants (of degree 9) must lie in the plane P. However, the remaining 4 control points use the three dimensions in order to satisfy the PH conditions.

It is known [8, 22] that there are four planar C^2 (non-spurious) PH interpolants of degree 9 for planar data. The following theorem shows how these interpolants are reproduced by the general spatial construction.

Theorem 3.11. *For given* C^2 *Hermite data contained in a plane* $P \subset \mathbb{R}^3$*, the interpolants*

$$\mathbf{p}_{[0,0,0,0]}(t), \quad \mathbf{p}_{[\pi,0,0,0]}(t), \quad \mathbf{p}_{[0,0,0,\pi]}(t), \quad \mathbf{p}_{[\pi,0,0,\pi]}(t) \tag{3.18}$$

are contained in P*. Moreover, if any other interpolant* $\mathbf{p}_\Phi$ *is contained in* P*, it is identical with one of interpolants* (3.18)*.*

Proof. We can suppose without loss of generality that $P = \mathbb{Q}_{ij}$ and that the data are in a standard position. Then the control points $\mathcal{A}_i$ constructed in the Algorithm 3.1 with parameter values

$$\tau_1 = \tau_3 = 0, \quad \theta_0, \theta_4 \in \{0, \pi\}$$

are contained in $\mathbb{Q}_{ij}$ due to Lemma 2.8 and from the same lemma follows that the hodograph will be contained in $\mathbb{Q}_{\mathbf{ij}}$, too. Therefore the constructed PH curves are planar.

Moreover, restricted to $\mathbb{Q}_{\mathbf{ij}}$, the characterization mapping (2.19) is isomorphic to the complex squaring, which is a representation of planar PH curves [5]. Then the equations (2.23)–(2.31) and (3.3) become the complex equations due to Lemma 2.8 and are identical with the complex equations describing C^2 Hermite interpolation problem in the plane - see [22, equations (4)–(7)]. For this reason, the four interpolants (3.18) reproduce the four planar interpolants described in [22, Table 2]. As there are no other (non-spurious) planar interpolants of planar data [22], any other interpolant $\mathbf{p}_\Phi$ must coincide with one of (3.18). □

3.4. **Reducing the degree of the interpolants.** In principle, the four parameters $[\theta_0, \tau_1, \tau_3, \theta_4]$ could be used to reduce the degree of the PH interpolants. More precisely, one might try to reduce the degree of the quaternion–valued preimage $\mathcal{A}_\Phi(t)$ from 4 to 3, order to obtain interpolants of degree 7. The conditions of degree reduction lead to four equations, which can – in some cases – be solved to determine suitable values of the parameters $\theta_0, \tau_1, \tau_3, \theta_4$.

However, the system of equations for the parameters $\theta_0, \tau_1, \tau_3, \theta_4$ is highly nonlinear and we were not able to obtain an explicit characterization of the set of data admitting PH interpolants of degree 7. Let us demonstrate the complexity of this problem on the following example. Consider the boundary data

$$\begin{array}{rclrclrcl} \mathbf{p}_b & = & [0,0,0], & \mathbf{v}_b & = & [3,4,0], & \mathbf{a}_b & = & [0,0,0], \\ & & & \mathbf{v}_e & = & [3,-4,0], & \mathbf{a}_e & = & [0,0,0], \end{array} \tag{3.19}$$

while the position $\mathbf{p}_e$ of the end-point remains free. This is a particularly simple set of boundary data, since both boundary accelerations vanish. For these data we were able to characterize the values of $\mathbf{p}_e$ which admit a degree 7 PH interpolant.

The control points $\mathcal{A}_0, \mathcal{A}_1, \mathcal{A}_3, \mathcal{A}_4$ can be determined from (3.19), depending on 4 free parameters $\theta_0, \tau_1, \tau_3, \theta_4$. If the degree of the preimage is to be reduced to 3 then the control point $\mathcal{A}_2$ is also determined as $\mathcal{A}_2 = (-\mathcal{A}_0 + 4\mathcal{A}_1 + 4\mathcal{A}_3 - \mathcal{A}_4)/6$ and the whole preimage depends on $\theta_0, \tau_1, \tau_3, \theta_4$. It can be shown that the resulting PH curve depends only on τ_1, τ_3 and goniometric functions of the difference $\theta_4 - \theta_0$. Using the standard rational parameterization $\cos(\theta_4 - \theta_0) = (1 - \tau^2)/(1 + \tau^2)$ and $\sin(\theta_4 - \theta_0) = 2\tau/(1 + \tau^2)$ we obtain a rational parametric expression of all possible end points positions $\mathbf{p}_e$.

By using elimination techniques from computer algebra we were able to derive (with a help of a computer algebra tool) the implicit equation of the boundary of the set of all end point positions. The algebraic degree of the boundary is 28, and its implicit equation contains 2,360 terms. It is therefore virtually impossible, even for these simple data, to understand the geometry of the set of possible positions of $\mathbf{p}_e$. For general data, the problem becomes even more complex and we were even not able to obtain an implicit equation of the boundary.

As another serious problem with degree reduction, the PH interpolants of degree 7 do not preserve planarity of the data. Only for very exceptional planar data one of the four planar interpolants (see Theorem 3.11) has degree 7. As an example, consider the boundary data, (with undetermined position of $\mathbf{p}_e$)

$$\begin{array}{rclrclrcl} \mathbf{p}_b & = & [0,0,0], & \mathbf{v}_b & = & [3,4,0], & \mathbf{a}_b & = & [2,3,0], \\ & & & \mathbf{v}_e & = & [3,-4,0], & \mathbf{a}_e & = & [3,2,0]. \end{array}$$

A careful inspection of the non-linear system of equations reveals that only for 4 discrete positions of the end point,

$$\mathbf{p}_e \in \left\{ \left[\tfrac{2497}{700}, -\tfrac{1081}{21000}\right], \left[\tfrac{2497}{700}, \tfrac{1577}{12000}\right], \left[\tfrac{1649}{2100}, -\tfrac{5357}{28000}\right], \left[\tfrac{1649}{2100}, \tfrac{1243}{7000}\right] \right\},$$

one of the planar PH interpolants has degree 7 instead of 9. Hence, planar PH interpolants of degree 7 to planar data do not always exist.

Due to these very complicated existence conditions and the lack of planarity preservation, the degree 7 PH interpolants do not seem to be suitable for applications. If the high degree 9 causes problems, one could instead design an interpolation scheme using two PH curves of degree 7, or three PH curves of degree 5, joined together with C^2 continuity. Such schemes might be a subject of future research.

4. Qualitative analysis of the interpolants

In this section we give a qualitative analysis of the system of PH quintic interpolants, in order to identify the 'best' values of the parameter vector Φ_0. These parameters yield the interpolants suitable for applications.

4.1. **Asymptotic behavior.** In order to fix the free parameters $\theta_0, \theta_4, \tau_1, \tau_3$, we will now study the asymptotic behavior of the solutions $\mathbf{p}_\Phi(t)$. More precisely, we assume that the C^2 Hermite data are taken from a small segment of an analytical curve, and we investigate the asymptotic behavior of the solutions for decreasing step-size.

We assume that the curve is given by its Taylor expansion. Without loss of generality,

$$\mathbf{C}(T) = (T + \sum_{i=2}^{\infty} \frac{x_i}{i!} T^i,\ \sum_{i=2}^{\infty} \frac{y_i}{i!} T^i,\ \sum_{i=2}^{\infty} \frac{z_i}{i!} T^i)^\top \tag{4.1}$$

with arbitrary coefficients $x_i, y_i, z_i, i = 2, 3, \ldots$.

For any step–size h we pick the segment $\mathbf{c}(t) = \mathbf{C}(ht)$, $t \in [0, 1]$. This segment has the expansion

$$\mathbf{c}(t) = (th + \sum_{i=2}^{\infty} \frac{x_i}{i!} t^i h^i,\ \sum_{i=2}^{\infty} \frac{y_i}{i!} t^i h^i, \sum_{i=2}^{\infty} \frac{z_i}{i!} t^i h^i)^\top. \tag{4.2}$$

Now we interpolate the C^2 Hermite boundary data at the points $\mathbf{c}(0) = \mathbf{C}(0)$ and $\mathbf{c}(1) = \mathbf{C}(h)$. Depending on the interval size h, different PH curves interpolating the data behave as described in the following theorem.

Theorem 4.1. *The error of the PH interpolation*

$$E = \max_{t \in [0,1]} ||\mathbf{c}(t) - \mathbf{p}_\Phi(t)|| \tag{4.3}$$

converges to 0 *for* $h \to 0$ *if and only if* $\tau_1 = \tau_3 = 0$. *Moreover, if* $\theta_0 = \theta_4 = 0$, *then* $E = \mathcal{O}(h^6)$. *Otherwise* $E = \mathcal{O}(h^1)$.

Proof. The proof consists in evaluating the power series of all quantities occurring in the interpolation process with respect to the step size h. This can be done by a suitable computer algebra tool. Due to the space limitation and the complexity of the expressions, we show only the leading terms of certain quantities, in order to illustrate the idea of our approach.

We derive the Taylor expansions of the Hermite boundary data at $t = 0$ and $t = 1$ of the curve (4.2),

$$\begin{aligned}
\mathbf{p}_b &= \begin{pmatrix} 0 \\ 0 \\ 0 \end{pmatrix}, \qquad \mathbf{p}_e = \begin{pmatrix} h + \frac{1}{2}x_2h^2 + \frac{1}{6}x_3h^3 + \dots \\ \frac{1}{2}y_2h^2 + \frac{1}{6}y_3h^3 + \dots \\ \frac{1}{2}z_2h^2 + \frac{1}{6}z_3h^3 + \dots \end{pmatrix}, \\
\mathbf{v}_b &= \begin{pmatrix} h \\ 0 \\ 0 \end{pmatrix}, \qquad \mathbf{v}_e = \begin{pmatrix} h + x_2h^2 + \frac{1}{2}x_3h^3 + \dots \\ y_2h^2 + \frac{1}{2}y_3h^3 + \dots \\ z_2h^2 + \frac{1}{2}z_3h^3 + \dots \end{pmatrix}, \\
\mathbf{a}_b &= \begin{pmatrix} x_2h^2 \\ y_2h^2 \\ z_2h^2 \end{pmatrix}, \quad \mathbf{a}_e = \begin{pmatrix} x_2h^2 + x_3h^3 + \frac{1}{2}x_4h^4 + \dots \\ y_2h^2 + y_3h^3 + \frac{1}{2}y_4h^4 + \dots \\ z_2h^2 + z_3h^3 + \frac{1}{2}z_4h^4 + \dots \end{pmatrix}.
\end{aligned} \tag{4.4}$$

This data can be transformed into a standard position by the rotation U given by the matrix

$$\begin{pmatrix} 1 - \frac{{y_2}^2 + {z_2}^2}{8}h^2 + \dots & \frac{y_2}{2}h + \frac{y_3 - y_2x_2}{4}h^2 + \dots & \frac{z_2}{2}h + \frac{z_3 - z_2x_2}{4}h^2 + \dots \\ -\frac{y_2}{2}h - \frac{y_3 - y_2x_2}{4}h^2 + \dots & 1 - \frac{{y_2}^2}{8}h^2 + \dots & 0 \\ -\frac{z_2}{2}h - \frac{z_3 - z_2x_2}{4}h^2 + \dots & -\frac{z_2y_2}{4}h^2 + \dots & 1 - \frac{{z_2}^2}{8}h^2 + \dots \end{pmatrix}.$$

Then we compute the Taylor expansions of the control points of the preimage for the transformed data $U(\mathbf{p}_b), U(\mathbf{p}_e), U(\mathbf{v}_b), U(\mathbf{v}_e), U(\mathbf{a}_b), U(\mathbf{a}_e)$. Using the formula (3.1) we derive in the Step 1 of Algorithm 3.1 the expansions of the control points $\mathbf{h}_0$, $\mathbf{h}_1$, $\mathbf{h}_7$ and $\mathbf{h}_8$. Then using (2.13), we derive in the Step 2 the expansions of the control points $\mathcal{A}_0$ and $\mathcal{A}_4$

$$\mathcal{A}_0 = \begin{pmatrix} -\sin(\theta_0)\sqrt{h} + \mathcal{O}\left(h^{3/2}\right) \\ \cos(\theta_0)\sqrt{h} + \mathcal{O}\left(h^{3/2}\right) \\ \mathcal{O}\left(h^{3/2}\right) \\ \mathcal{O}\left(h^{3/2}\right) \end{pmatrix} \quad \mathcal{A}_4 = \begin{pmatrix} -\sin(\theta_4)\sqrt{h} + \mathcal{O}\left(h^{3/2}\right) \\ \cos(\theta_4)\sqrt{h} + \mathcal{O}\left(h^{3/2}\right) \\ \mathcal{O}\left(h^{3/2}\right) \\ \mathcal{O}\left(h^{3/2}\right) \end{pmatrix}. \tag{4.5}$$

Using formula (2.10) we derive in the Step 3 the expansions of the control points $\mathcal{A}_1$ and $\mathcal{A}_3$

$$\mathcal{A}_1 = \begin{pmatrix} \frac{\tau_1\cos(\theta_0)}{\sqrt{h}} + \mathcal{O}\left(\sqrt{h}\right) \\ \frac{\tau_1\sin(\theta_0)}{\sqrt{h}} + \mathcal{O}\left(\sqrt{h}\right) \\ \mathcal{O}\left(\sqrt{h}\right) \\ \mathcal{O}\left(\sqrt{h}\right) \end{pmatrix} \quad \mathcal{A}_3 = \begin{pmatrix} \frac{\tau_3\cos(\theta_4)}{\sqrt{h}} + \mathcal{O}\left(\sqrt{h}\right) \\ \frac{\tau_3\sin(\theta_4)}{\sqrt{h}} + \mathcal{O}\left(\sqrt{h}\right) \\ \mathcal{O}\left(\sqrt{h}\right) \\ \mathcal{O}\left(\sqrt{h}\right) \end{pmatrix}. \tag{4.6}$$

At this stage we can already fix the free parameters τ_1, τ_3. For $h \to 0$ the curve $\mathbf{c}(t)$ converges to $(0,0,0)^\top$ on the whole interval $[0,1]$. Therefore, if the error (4.3) should converge to 0, the curve $\mathbf{p}_\Phi(t)$ must converge to to $(0,0,0)^\top$ on the whole interval $[0,1]$, too. Hence, its hodograph must converge to $(0,0,0)^\top$ and the preimage $\mathcal{A}_\Phi(t)$ must converge to $(0,0,0,0)^\top$ on the interval $[0,1]$. This implies that the control points of the preimage, in particular $\mathcal{A}_1$ and $\mathcal{A}_3$ have to converge to $(0,0,0,0)^\top$, and therefore τ_1 and τ_3 must vanish.

After setting $\tau_1 = \tau_3 = 0$ we derive in the Step 4 the expansion of the control point $\mathcal{A}_2$

$$\mathcal{A}_2 = \begin{pmatrix} \frac{5\sin(\theta_4)+5\sin(\theta_0)}{4}\sqrt{h} + \mathcal{O}\left(h^{3/2}\right) \\ \frac{\sqrt{170+26\cos(\theta_0-\theta_4)}-5\cos(\theta_0)-5\cos(\theta_4)}{4}\sqrt{h} + \mathcal{O}\left(h^{3/2}\right) \\ \mathcal{O}\left(h^{3/2}\right) \\ \mathcal{O}\left(h^{3/2}\right) \end{pmatrix}. \tag{4.7}$$

Finally, in the Step 5 using (2.25)–(2.29) we get the expansions of the remaining control points $\mathbf{h}_2$, $\mathbf{h}_3$, $\mathbf{h}_4$, $\mathbf{h}_5$ and $\mathbf{h}_6$ of the hodograph and using (2.32) the expansions of the control points of the PH curve and of the PH curve $\mathbf{p}_\Phi(t)$ itself. Comparing the expansion of $\mathbf{p}_\Phi(t)$ with the expansion (4.2) of $\mathbf{c}$ we obtain

$$\mathbf{p}_\Phi(t) - \mathbf{c}(t) = \begin{pmatrix} \left([X-5Y-9]\,t^3 + \frac{1}{2}\,[3X-19Y-23]\,t^4 + \sum_{i=5}^{9} r_i t^i\right)h + \mathcal{O}\left(h^2\right) \\ \mathcal{O}\left(h^2\right) \\ \mathcal{O}\left(h^2\right) \end{pmatrix}, \tag{4.8}$$

where

$$X = \cos(\theta_0)\sqrt{170 + 26\,\cos(\theta_0 - \theta_4)} \text{ and } Y = \cos(\theta_0 - \theta_4)\,. \tag{4.9}$$

Therefore the error (4.3) converges to 0 only as $\mathcal{O}(h)$ unless

$$X - 5Y - 9 = 0 \text{ and } 3X - 19Y - 23 = 0, \tag{4.10}$$

which holds only for $X = 14$ and $Y = 1$ implying $\theta_0 = \theta_4 = 0$.

After setting $\theta_0 = \theta_4 = 0$ the Taylor expansion of $\mathbf{p}_\Phi(t)$ simplifies enormously and matches the Taylor expansion of $\mathbf{c}(t)$ up to h^5. □

Theorems 3.10, 3.11 and 4.1 imply that the interpolant obtained for the parameter vector $\Phi = [0, 0, 0, 0]$ is particularly well suited for applications. We will denote this interpolant as $\mathbf{p}_0(t)$ and summarize its properties in the following theorem.

Theorem 4.2. *The C^2 Hermite PH interpolant $\mathbf{p}_0(t)$ preserves planarity of the input data, is invariant under all orthogonal transformation, under scaling and under reversion of the input data and has approximation order 6.*

5. Applications

We apply the previous results in order to design an algorithm converting any analytical curve into a piecewise PH curve of degree 9. This conversion is then used for approximation of pipe surfaces.

5.1. **Conversion of analytical curves.** The result described in Theorem 4.1 allows us to design an algorithm for the conversion of any analytical curve into a piecewise PH curve. Let the parameter domain of the analytical curve be $[0, 1]$. We split this interval into 2^n subintervals $[\frac{i}{2^n}, \frac{i+1}{2^n}]$, $i = 0..2^n - 1$. For each subinterval we construct the PH Hermite interpolant $\mathbf{p}_0(t)$ and obtain a C^2 continuous piecewise PH curve of degree 9. If the error from the original analytical curve is not sufficiently small, we continue the subdivision. Due to the Proposition 4.1, the error will converge to 0 as $\mathcal{O}\left(\frac{1}{64^n}\right)$ under subdivision.

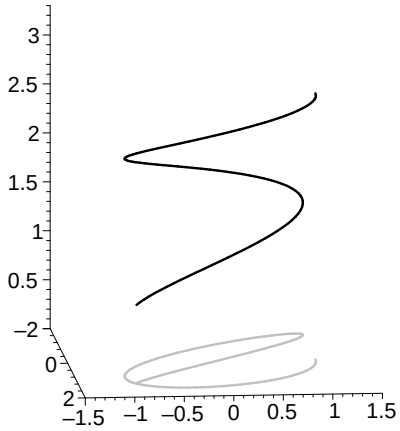

FIGURE 3. Analytical curve with its projection into the xy plane (gray line).

#Segments	Error	Ratio	#Segments	Error	Ratio
1	1.449		32	$1.144\,10^{-5}$	27.33×
2	$8.816\,10^{-1}$	1.643×	64	$2.287\,10^{-7}$	50.04×
4	$6.963\,10^{-2}$	12.66×	128	$3.770\,10^{-9}$	60.65×
8	$7.243\,10^{-3}$	9.613×	256	$6.027\,10^{-11}$	62.56×
16	$3.128\,10^{-4}$	23.16×	512	$9.436\,10^{-13}$	63.87×

TABLE 1. The error of piecewise PH approximation via Hermite interpolation.

The relatively high rate of convergence is demonstrated by the following example. Figure 3 shows the segment of the analytical curve

$$\mathbf{c}(t) = (1.5\sin(7.2t), \cos(9t), e^{\cos(1.8t)})^{\top}, t \in [0,1]. \tag{5.1}$$

We construct the PH Hermite interpolants for the whole segment and the piecewise PH interpolants obtained after splitting the parameter into 2, 4, 8, ... ,2^9 subintervals (the shape of first four piecewise interpolants can be seen from the associated pipe surfaces shown on the Figure 4). The maximal approximation error and its improvement (ratio) in each step are shown in Table 1. The ratio of the improvement is closer and closer to 64. As we have observed in [23], in the case of C^1 interpolation the ratio of the improvement converges to 16.

Clearly, instead of the simple uniform subdivision, using an adaptive subdivision scheme would reduce the number of segments.

5.2. **Approximation of pipe surfaces.** PH curves possess a simple low degree rational adapted frame, which has been called the Euler-Rodrigues frame [3]. Based on this construction, Farouki proposed a rational approximation of the rotation minimizing frame for any space PH curve [14].

Both frames can be used for the approximation of pipe surfaces, or – more generally – of sweep surfaces. First we convert a given analytical curve into a piecewise PH curve using the algorithm of section 5.1 and then we construct a pipe surface

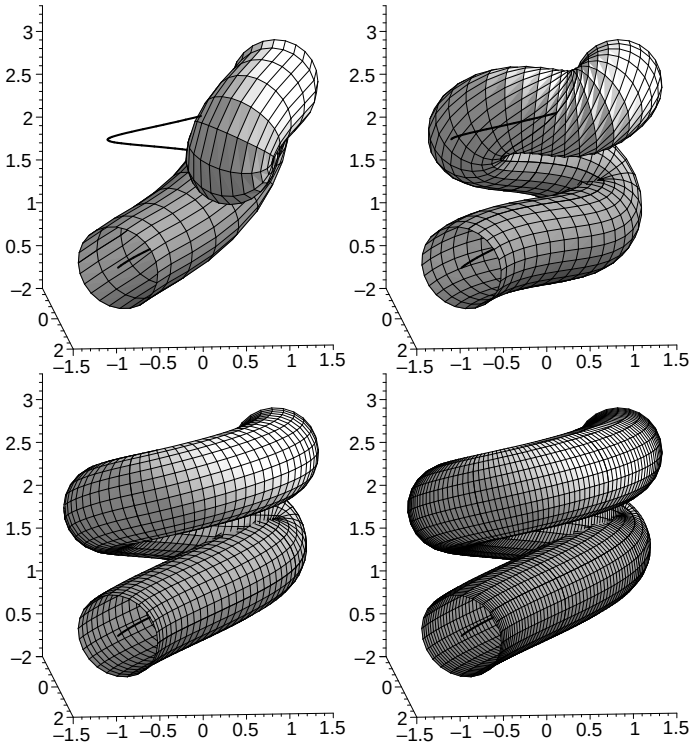

FIGURE 4. Analytical curve (5.1) and rational approximations of the associated pipe surface with the radius $0,5$. Piecewise PH curves of degree 9 constructed in the paragraph 5.1 and composed of 1, 2, 4 and 8 segments are used as spine curves of the approximations.

for this PH curve. It can be shown, that the error of the pipe surface approximation behaves as $\mathcal{O}(h^5)$ (see [23] for similar result using C^1 Hermite interpolation).

As an example, Figure 4 shows approximations of the pipe surface with the spine curve $\mathbf{c}(t)$ defined by (5.1). Piecewise PH curves with 1, 2, 4 and 8 segments are used as spine curves of the rational pipe surfaces.

6. Conclusion

We have solved the C^2 Hermite interpolation problem by space Pythagorean Hodograph curves. As observed in our previous research [21], the interpolation by curves of degree 7 leads to a highly nonlinear system of equations which does not always produce real solutions (see also section 3.4 of this paper). In the present paper we have used PH curves of degree 9 and we have shown that a four–dimensional family of interpolants always exist and can be constructed explicitly.

By using a standard position and by fixing the four free parameters we have identified the C^2 Hermite interpolant $\mathbf{p}_0(t)$ (see Theorem 4.2) which preserves planarity of the input data, is invariant under all orthogonal transformation, under scaling and under reversion of the input data and has approximation order 6. Therefore, it is the most suitable for applications.

We have explicitly addressed its use for the conversion of analytical curves into piecewise PH curves of degree 9 and for approximation of pipe surfaces. Another natural application of the C^2 Hermite interpolation is an acceleration smoothening of tool paths described in the standard G-code, which is a subject of our current research and of industrial tests performed by Dr. Elmar Wings at the CNC department of ProCom GmbH (Aachen, Germany).

In our constructions, we have used quaternion calculus, as usual for the description of space PH curves, but we have clarified and simplified the quaternion manipulations by introducing the commutative multiplication $\star$ (see Def. 2.2) essential for the representation of PH curves. This multiplication also allowed us to understand planar PH curves as embedded among the space ones via the inclusion

$$(\mathbb{C}, \cdot) \cong (\mathbb{Q}_{ij}, \star) \subset (\mathbb{Q}, \star) \tag{6.1}$$

(see Def. 2.7, Lemma 2.8 and Theorem 3.11). This approach is very general and can be exploited for a systematic unified treatment of space and planar PH curves.

Acknowledgment. The first author was supported through grant P17387-N12 of the Austrian Science Fund (FWF).

References

[1] M.-H. Ahn, G.-I. Kim and C.-N. Lee, Geometry of root-related parameters of PH curves. Appl. Math. Lett. **16** (2003), no. 1, 49–57.
[2] H.I. Choi, D.S. Lee and H.P. Moon (2002), Clifford algebra, spin representation, and rational parameterization of curves and surfaces. Adv. Comput. Math. 17, 5-48.
[3] H.I. Choi, C.Y. Han, Euler Rodrigues frames on spatial Pythagorean-hodograph curves, Comput. Aided Geom. Design 19 (2002) 603–620.
[4] R. Dietz, J. Hoschek, B. Jüttler, An algebraic approach to curves and surfaces on the sphere and on other quadrics, Comp. Aided Geom. Design 10 (1993), 211-229.
[5] R.T. Farouki (1994), The conformal map $z \to z^2$ of the hodograph plane. Comp. Aided Geom. Design 11, 363-390.
[6] R.T. Farouki and T. Sakkalis, Pythagorean-hodograph space curves, Adv. Comput. Math. 2 (1994) 41-66.
[7] R.T. Farouki and C.A. Neff (1995), Hermite interpolation by Pythagorean-hodograph quintics. Math. Comput. 64, 1589-1609.
[8] R. T. Farouki, J. Manjunathaiah and S. Jee (1998), Design of rational cam profiles with Pythagorean-hodograph curves. Mech. Mach. Theory 33, 669-682.
[9] R. T. Farouki and K. Saitou and Y-F. Tsai (1998), Least-squares tool path approximation with Pythagorean-hodograph curves for high-speed CNC machining. The Mathematics of Surfaces VIII, Information Geometers, Winchester, 245-264.
[10] R. T. Farouki, M. al-Kandari and T. Sakkalis (2002), Hermite interpolation by rotation-invariant spatial Pythagorean-hodograph curves., Adv. Comput. Math. 17, 369-383.
[11] R. T. Farouki, M. al-Kandari and T. Sakkalis (2002), Structural invariance of spatial Pythagorean hodographs, Comp. Aided Geom. Design 19, 395-407.
[12] R.T. Farouki (2002), Pythagorean hodograph curves, in G. Farin, J. Hoschek and M.-S. Kim (eds.), Handbook of Computer Aided Geometric Design, North-Holland, Amsterdam, 405–427.
[13] R.T. Farouki, C. Manni, A. Sestini (2003), Spatial C^2 PH quintic splines. Curve and surface design (Saint-Malo, 2002), 147–156, Mod. Methods Math., Nashboro Press.
[14] R.T. Farouki, C. Y. Han (2003), Rational approximation schemes for rotation-minimizing frames on Pythagorean hodograph curves, Computer Aided Geometric Design 20, 435-454.
[15] R.T. Farouki, C.Y. Han, C. Manni, A. Sestini (2004), Characterization and construction of helical polynomial space curves, J. Comput. Appl. Math. 162, no. 2, 365–392.
[16] J. Hoschek and D. Lasser (1996), Fundamentals of Computer Aided Geometric Design, AK Peters, Wellesley MA.
[17] B. Jüttler and C. Mäurer (1999), Cubic Pythagorean Hodograph Spline Curves and Applications to Sweep Surface Modeling, Comp.–Aided Design 31, 73–83.

[18] B. Jüttler (2001), Hermite interpolation by Pythagorean hodograph curves of degree seven. Math. Comp. 70, 1089–1111.
[19] J.B. Kuipers (1999), Quaternions and rotation sequences. Princeton University Press.
[20] H.P. Moon, R.T. Farouki and H.I. Choi (2001), Construction and shape analysis of PH quintic Hermite interpolants, Comp. Aided Geom. Design 18, 93-115.
[21] Z. Šír (2003), Hermite interpolation by space PH curves. Proceedings of the 23rd Conference on Geometry and Computer Graphics, University Plzeň, 193-198.
[22] Z. Šír and B. Jüttler (2005), Constructing acceleration continuous tool paths using pythagorean hodograph curves. Mech. Mach. Theory. 40(11), 1258-1272.
[23] Z. Šír and B. Jüttler (2005), Spatial Pythagorean Hodograph Quintics and the Approximation of Pipe Surfaces, in R. Martin, H. Bez and M. Sabin, editors, The Mathematics of Surfaces XI, Springer, 364-380.
[24] D.S. Meek and D.J. Walton (1997), Geometric Hermite interpolation with Tschirnhausen cubics, Journal of Computational and Applied Mathematics 81, 299-309.
[25] D.J. Walton and D.S. Meek (2004), A generalisation of the Pythagorean hodograph quintic spiral. J. Comput. Appl. Math. 172, no. 2, 271–287.

Johannes Kepler University, Institute of Applied Geometry, Altenberger Str. 69, 4040 Linz, Austria.
E-mail address: {zbynek.sir,bert.juettler}@jku.at